Journal of Biomedical Optics

SPIEDigitalLibrary.org/jbo

Broadband absorption spectroscopy of turbid media using a dual step steady-state method

Florian Foschum
Alwin Kienle

SPIE

Broadband absorption spectroscopy of turbid media using a dual step steady-state method

Florian Foschum and Alwin Kienle
Institut für Lasertechnologien in der Medizin und Meßtechnik an der Universität Ulm, Helmholtzstraße 12, 89081 Ulm, Germany

Abstract. We present a method for the determination of the absorption coefficient of turbid media in a broad wavelength range with high spectral resolution using a dual step method. First, the reduced scattering coefficient is determined for a few wavelengths with spatially resolved reflectance measurements. The reduced scattering coefficient for the intermediate wavelengths is interpolated by fitting a power law. Second, the absorption coefficient is obtained from measurements of the total reflectance using the a priori knowledge of the reduced scattering coefficient. By applying a white light source and a spectrometer to measure the total reflectance, the absorption coefficient is determined with a high spectral resolution. The methodology is verified by comparing the absorption coefficients determined by the spatially resolved reflectance measurements with those obtained by the dual step method. The influence of an unknown refractive index and phase function on the determination of the optical properties is investigated. In addition, the optical properties of Intralipid/ink phantoms and the fat layer of porcine rind were determined. The absorption coefficient of the investigated phantoms varying by four orders of magnitude could be determined with an average error of less than 10%. [DOI: 10.1117/1.JBO.17.3.037009]

Keywords: spatially resolved reflectance; total reflectance; optical properties; absorption spectrum; turbid media; intralipid.

Paper 11356 received Jul. 12, 2011; revised manuscript received Oct. 27, 2011; accepted for publication Jan. 11, 2012; published online Apr. 6, 2012.

1 Introduction

Calculations of the light propagation in turbid media depend on the optical properties and, thus, their precise determination is important, such as for applications in biophotonics. In addition, the spectrally resolved absorption coefficient carries information about the ingredients of the turbid medium, which can be used for process control. In the past, different methods measuring the reflected light from turbid samples were used for the determination of the absorption and the reduced scattering coefficients. Using methods like the measurement of the time-resolved reflectance,[1,2] the frequency-domain reflectance[3–5] or the spatially resolved reflectance,[6–10] both coefficients can be obtained. As most of these methods determine the optical properties only for a few wavelengths, the spectral information cannot be fully exploited. However, the spectral resolution can be included in the fiber-based spatially-resolved reflectance if a spectrometer is used for detection.[11,12] Alternatively, the measurement of the frequency-domain reflectance at several wavelengths can be combined with the steady-state reflectance determined at one distance with a high-spectral resolution.[13]

In this work, we present a method for the determination of the absorption coefficient of homogeneous, quasi semi-infinite turbid media combining the measurement of the spatially resolved reflectance (SRR) and of the total reflectance (TR). Using a recently described SRR setup,[14] the reduced scattering coefficient μ_s' and absorption coefficient μ_a is determined in the spectral range from 450 to 950 nm. This measurement is especially sensitive to the determination of μ_s'. As the measurements have to be performed successively, only a poor wavelength resolution can be obtained within a reasonable measurement time. Based on the flat curve shape of the μ_s' spectrum of many turbid media the dependence of the reduced scattering coefficient versus wavelength can often be described by a power law. Therewith μ_s' can be interpolated for any wavelength. In a second step the scattered light from an illuminated sample in a certain direction is measured with the TR method, achieving a high spectral resolution with a white light source for illumination and a spectrometer as a detector. As we cannot distinguish between scattering and absorption with this method, we use the a priori information of the reduced scattering coefficient measured with the SRR method to determine the absorption coefficient. The evaluation is performed by means of Monte Carlo (MC) simulations considering the setup geometry. The absorption coefficients obtained with the dual step method can be compared with those determined within the SRR method. Especially in turbid tissue, for which the phase function and the refractive index is often not exactly known, this helps confirm the measured coefficients.

The scope of this technique is the determination of the optical properties of homogeneous media, which can be assumed to be semi-infinite. For example, in the process control, as well as for characterization of optical phantoms, this geometry is often applicable.

The literature describes another two-step method for determination of the optical properties in the steady state domain. Patterson et al.[15] presented a combination of a spatially resolved and a total reflectance method for a single wavelength. The total reflectance was measured using an integrating sphere accepting the re-illumination of the sample by the integrating sphere.

Address all correspondence to: Florian Foschum, Institut für Lasertechnologien in der Medizin und Meßtechnik an der Universität Ulm, Helmholtzstraße 12, 89081 Ulm, Germany. Tel: +49 0731 1429 779; E-mail: florian.foschum@ilm.uni-ulm.de.

0091-3286/2012/$25.00 © 2012 SPIE

The reflectance was analyzed by means of a solution of the diffusion theory. Wilson et al.[16] used the same setup again at a single wavelength and improved the theory using MC simulations, but they did not regard the exact geometry of the setup in the simulations.

2 Experimental Setup

2.1 *Spatially Resolved Reflectance*

In our recent article[14] a fully automated SRR spectrometer is described. A CCD camera is used to measure the intensity profile on the surface of a point-like illuminated sample at distances up to 25 mm with a resolution of approximately 90 μm. We showed that it is very important to take the characteristics of the setup into account, for example, the optical transfer function of the system and the dependence of the background on the time elapsed since the last picture. Systematic errors caused by using the diffusion theory to determine the optical properties were estimated. Using liquid phantoms we showed with this setup that it is possible to determine the reduced scattering and absorption coefficients with an error smaller than 6% and 20%, respectively.

2.2 *Total Reflectance*

In the TR method the sample is illuminated by applying a white light source. A scheme of the setup is shown in Fig. 1. A tungsten halogen light source is coupled into a optical fiber bundle (∅ 6 mm) where the sample-sided end is imaged perpendicularly onto the surface of the sample. The incident power on the sample surface is about 60 mW for the whole spectrum. An aperture between the fiber bundle and the imaging lens ($f = 50$ mm, achromatic, VIS AR coated) avoids the illumination of the lens mount. The spot size on the surface is 11 mm in diameter with a maximum angle of incidence of 2 deg with respect to the surface normal. The light, scattered from all positions at the surface in the direction of the detector, is measured using a spectrometer (BTC112E TE, Polytec GmbH, Waldbronn, Germany). With this spectrometer the reflectance can be measured from 450 to 1000 nm with a resolution of 0.5 nm. We used an integration time of 2.5 sec per scan and averaged the signal over 30 scans. The light is collected by means of a optical fiber (∅ 700 μm). To mix the angles coupled into the optical fiber a cosine corrector (CC-3, Ocean Optics, Dunedin, USA) is used in front of the optical fiber. The cosine corrector (∅ 5 mm) is mounted with an inclination angle of 20 deg with respect to the surface normal of the sample at a distance of 123 mm to the surface pointing to the center of the illumination spot. The use of the cosine corrector is essential, because the light from all locations of the sample surface has to be coupled into the optical fiber with almost the same probability and angular distribution. The specular reflex of smooth sample surfaces is not detected, as it is back-reflected to the illumination optics. The incident light power is measured indirectly using a white standard (Spectralon SRS-75 to 010, Labsphere, North Sutton, USA) instead of the sample. For the perpendicularly illuminated reflectance standard the angular distribution of the reflected light was measured with a goniometer showing roughly a cosine dependence. The reflectance at the detection angle of 20 deg with respect to the surface normal of the sample was approximately 5% higher than the expected cosine dependence which is used in the evaluation process.

3 Theory

To analyze the TR measurements, we solved the radiative transfer equation (RTE) by means of MC simulations for the given setup geometry. For calculations of the light propagation in the turbid sample, a self-written MC code whose principles are similar to those described by Wang et al.[17] was used. A scheme of the setup geometry as regarded in the simulations is shown in Fig. 2. In these simulations the illumination spot was included by starting the photons equally distributed in a circle with a diameter of 11 mm. The incident cone was modeled by launching each photon with a randomly chosen starting angle between 0 and 2 deg with respect to the surface normal of the sample. The reflection on the surface is considered according to Fresnel's law. The sample geometry was assumed to be semi-infinite with a plain surface between the scattering and the non-scattering layer. To check the influence of the lateral surface boundaries absorbing borders are included at the position of the sample container. For the propagation procedure the medium is described by its reduced scattering coefficient μ_s', absorption coefficient μ_a, refractive index n and its phase function $p(\theta)$. For the phase function the Henyey-Greenstein[18] function was used, which includes as parameters the anisotropy factor g, defined as the average cosine of the scattering angles.

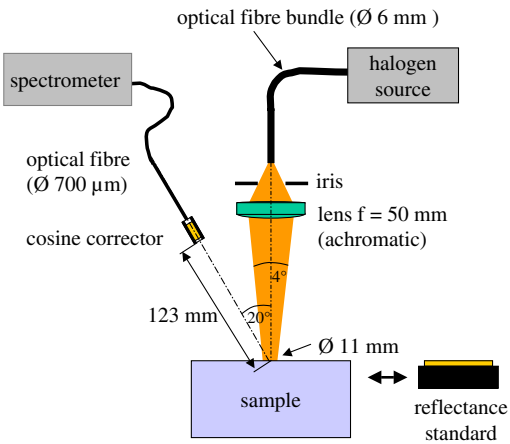

Fig. 1 Total reflectance setup for the determination of the absorption coefficient.

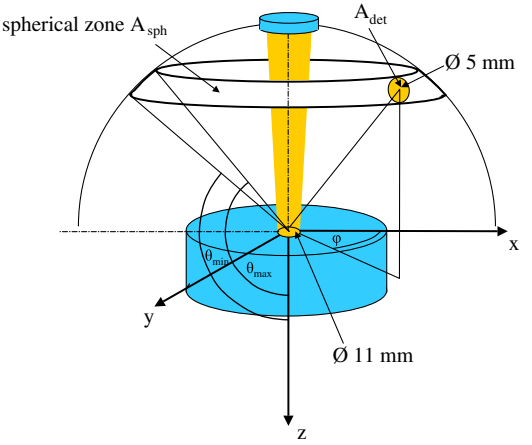

Fig. 2 Scheme of the setup geometry as used for the Monte Carlo simulations to analyze the measured data.

For all reflected photons we calculate (considering refraction) if they reach the detector. As the detector is relatively small only a few photons are collected by the detector and thereby the computing time is large. For isotropic light propagation in the sample and perpendicular light incidence the ϕ angle of the detector is irrelevant. Therefore we can collect all photons that hit the spherical zone containing the detector which leads to a better performance of the MC simulations.

The reflectance calculated from the simulation R_{sim} is the ratio of the detected photons within the spherical zone N_{sph} and the incident photons N_{total} as measured with the used detector considering the fraction of the area of the detector A_{det} and the area of the spherical zone A_{sph}

$$R_{\mathrm{sim}} = \frac{N_{\mathrm{sph}}}{N_{\mathrm{total}}} \frac{A_{\mathrm{det}}}{A_{\mathrm{sph}}}. \tag{1}$$

We note that if the spherical zone and the ratio of the areas are considered this is not the exact solution for the circular detector, as we create a trapezoidal area of the same size as the circular detector. But as the reflected light changes very slightly over the θ-angle this is an acceptable approximation.

In order to compare the reflectance of the simulation with that of the measurements the following steps have to be carried out to normalize the measurements. The reflectance of the sample R_{sam} is given by

$$R_{\mathrm{sam}} = \frac{P_{\mathrm{sam}}}{P_0}, \tag{2}$$

where P_{sam} is the measured power of the light reflected from the sample and P_0 the incident power. As the incident power is determined indirectly using a reflectance standard, the power reflected from this into the detector has to be calculated. Assuming a cosine dependence of the reflected light from the standard the reflected power per solid angle $P'(\theta)$ can be expressed as

$$P'(\theta) = \frac{1}{\pi} P_0 \cos(\theta). \tag{3}$$

Using the same spherical zone as in the simulations and considering the ratio of the areas leads to the power measured with the detector from the reflection standard P_{spec} of

$$P_{\mathrm{spec}} = P_0[\sin^2(\theta_{\mathrm{max}}) - \sin^2(\theta_{\mathrm{min}})] R_{\mathrm{spec}} F_{\mathrm{spec}} \frac{A_{\mathrm{det}}}{A_{\mathrm{sph}}} \tag{4}$$

by integrating $P'(\theta)$ between θ_{min} and θ_{max} of the spherical zone (see Fig. 2). Thereby the total reflection coefficient of the reflection standard R_{spec} is given by the manufacturer and F_{spec} is the measured deviation to the cosine dependence at the given detection angle (1.05). After inserting Eq. (4) into Eq. (2) the reflectance from the sample can be expressed by

$$R_{\mathrm{sam}} = \frac{P_{\mathrm{sam}}}{P_{\mathrm{spec}}} [\sin^2(\theta_{\mathrm{max}}) - \sin^2(\theta_{\mathrm{min}})] R_{\mathrm{spec}} F_{\mathrm{spec}} \frac{A_{\mathrm{det}}}{A_{\mathrm{sph}}}. \tag{5}$$

As the ratio of the areas $A_{\mathrm{det}}/A_{\mathrm{sph}}$ appears in the reflectance term of the simulation [Eq. (1)] as well as in the reflectance term of the measurement [Eq. (5)] it is not to necessary to calculate this ratio explicitly in order to compare measurement and simulation.

For the calibration a set of MC simulations was run. We fixed the reduced scattering coefficient to a certain value and calculated the reflectance measured within the spherical zone for absorption coefficients between 10^{-4} mm^{-1} $< \mu_a <$ 10 mm^{-1}. The refractive index was set to $n = 1.335$ and the anisotropy factor to $g = 0.8$ using the Henyey-Greenstein phase function as a mean value expected for measurements on Intralipid phantoms.[19] We repeated this procedure for different μ_s' that are given in Fig. 3 using 10^6 photons in the MC simulation. The ratio of μ_s'/μ_a is plotted against the simulated reflectance in Fig. 3.

Figure 3 shows that for a μ_s'/μ_a ratio smaller than 100 the reflectance is almost independent of the reduced scattering coefficient and depends just on the ratio of μ_s'/μ_a. For higher μ_s'/μ_a ratios the reflectance also depends on μ_s'. This means that for low absorption (high μ_s'/μ_a ratio) the actual reduced scattering coefficient in the phantom has to be regarded, whereas in media with a higher absorption (low μ_s'/μ_a ratio) one simulation with an arbitrary μ_s' is sufficient for the evaluation. This effect is caused by photons exiting the medium far from the source and entering the detector mainly within higher θ angles. For these photons the probability of hitting the detector is reduced. As a consequence, this effect reduces the reflectance especially if μ_a and μ_s' are both low, which can be observed in Fig. 3.

To analyze the measured reflectance values the simulated reflectance curves were fitted with a 13th order polynomial. With this polynomial the μ_s'/μ_a ratio for a measured reflectance can be quickly determined. As for lower μ_a the reflectance depends on the μ_s', we simulated the calibration curves for seven different reduced scattering coefficients between 0.5 mm^{-1} $< \mu_s' <$ 3.5 mm^{-1} and interpolated for the actual μ_s' in the sample. With the a priori information of the reduced scattering coefficient, we calculate the absorption coefficient of the turbid medium.

Based on the flat curve shape of the reduced scattering coefficient, it can even be extrapolated with good accuracy. In addition, in turbid media with high absorption it is often possible to find a spectral region in which the absorption is relatively low and where μ_s' can be determined using the SRR. By extrapolating μ_s' the absorption coefficient can then be determined for the whole spectral range.

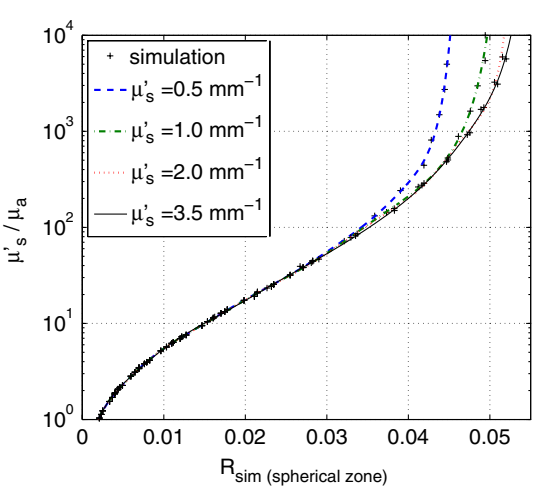

Fig. 3 Calibration curves for the determination of the optical properties simulated for the geometry of the described setup. The μ_s'/μ_a ratio (using a polynomial interpolation) is plotted versus the reflectance measured within the spherical zone for different reduced scattering coefficients.

3.1 *Other Approaches for Analysis*

Two alternative approaches can be used to obtain the TR. First, in order to improve the velocity of the MC simulations all photons reflected from the medium can be collected and the reflectance is calculated assuming a cosine dependence of the measured signal. Thereby the distance of the detector to the sample is assumed to be infinite and just the solid angle is considered. Second, an even faster approach to calculate the total reflectance of a turbid medium can be found within the diffusion theory (DT). The reflectance R_d can be expressed by

$$R_d = \frac{\alpha'}{1 + 2k(1-\alpha') + \left(1 - \frac{2k}{3}\right)\sqrt{3(1-\alpha')}} \tag{6}$$

following Patterson et al.[15] Thereby $\alpha' = (\mu_s')/(\mu_s'/\mu_a)$ is the transport albedo and $k = (1 + r_d)/(1 - r_d)$. The diffuse reflection coefficient is $r_d = -1.44n^{-2} + 0.71n^{-1} + 0.668 + 0.0636n$ with the refractive index n of the turbid medium. In Fig. 4 the two methods are compared to our method for a reduced scattering coefficient of $\mu_s' = 2.0\ \mathrm{mm}^{-1}$.

For low μ_s'/μ_a ratios there is almost no difference between the two MC methods. As for these ratios the photons propagate only short distances through the medium and leave it close to the source, so the influence of the detector geometry is low. The DT differs from both MC simulations as the DT is not valid for low μ_s'/μ_a ratios. For high μ_s'/μ_a ratios the MC simulation in which all photons are collected agrees with the DT as both methods consider all photons that leave the medium. In summary, the MC simulation including the setup geometry differs from both alternative methods and therefore the latter cannot be used for the evaluation of the absorption coefficient.

3.2 *Systematic Errors*

The refractive index and the phase function of turbid media are often unknown. For data analysis these coefficients have to be estimated. Furthermore, both coefficients depend on the wavelength. In Secs. 3.2.1 to 3.2.3 we investigate the influence on the determination of the absorption coefficient if a fixed refractive index, g-factor, and phase function are used for the spectral evaluation.

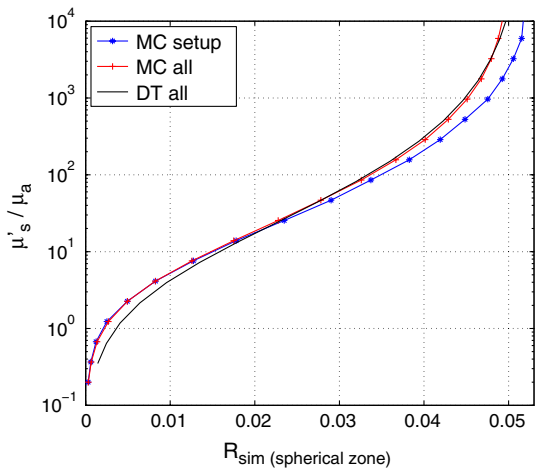

Fig. 4 Comparison of different methods for the evaluation of the absorption coefficient. The total reflectance calculated with the Monte Carlo method considering the setup geometry (MC setup) is shown next to the total reflectance calculated by Monte Carlo simulations where all photons are detected (MC all) and the solution of the diffusion theory (DT all).

3.2.1 *Refractive index*

For studying the influence of the unknown refractive index the reflectance was calculated with the MC simulation method considering the setup geometry. The parameters for the simulation were $\mu_s' = 1.0\ \mathrm{mm}^{-1}$ and $g = 0.75$ using the Henyey-Greenstein phase function. We run two sets of simulations with $\mu_a = 0.1\ \mathrm{mm}^{-1}$ and $\mu_a = 0.001\ \mathrm{mm}^{-1}$, respectively. In each set the refractive index of the medium was varied between $1.2 < n < 1.45$. The absorption coefficient was determined from these reflectance values using the calibration polynomial (see Sec. 3) of the simulations with $\mu_s' = 1.0\ \mathrm{mm}^{-1}$, $n = 1.33$ and an anisotropy factor of $g = 0.75$. The relative errors of the determined absorption coefficients are shown in Fig. 5. The study was repeated three times with 10^6 photons in all MC simulations. The error bars show the standard deviation of these three simulations. The relative error caused by the refractive index mismatch is almost independent of the absorption. For a deviation of 0.01 from the actual refractive index to the assumed one we obtained a relative error of about 2% in the determination of the absorption coefficient. Assuming a constant refractive index at all wavelengths for water-based phantoms in which the refractive index varies by 0.02 over the wavelength range between 450 and 950 nm we expect a maximum error of 4%.

3.2.2 *Asymmetry factor*

We calculated similar sets of simulations as in Sec. 3.2.1 fixing the refractive index to $n_M = 1.33$ and varying the asymmetry factor between $0.1 < g < 0.95$ assuming the Henyey-Greenstein function. An additional set of simulations using $\mu_a = 1\ \mathrm{mm}^{-1}$ was simulated. The relative errors are presented in Fig. 6. Here, a clear dependence on the absorption coefficient can be seen. If the absorption coefficient is large then the influence of the asymmetry factor on the determination of μ_a is also large. But as the asymmetry factor in biological tissue is usually between

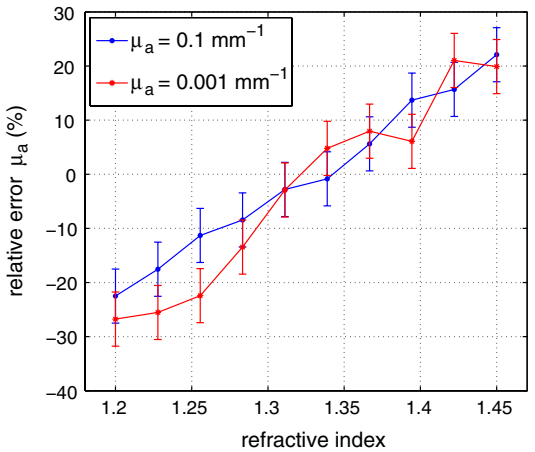

Fig. 5 Relative errors of the absorption coefficient if a wrong refractive index is assumed in the data analysis.

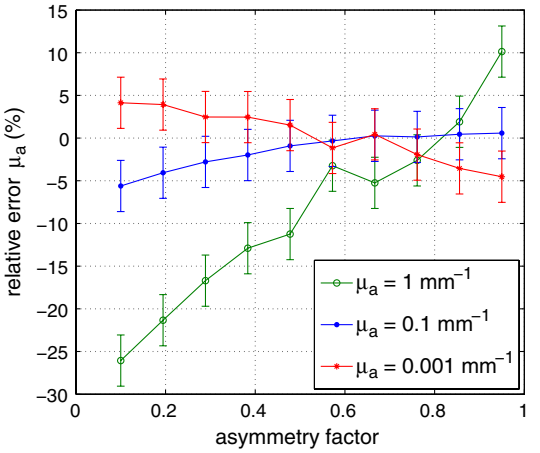

Fig. 6 Relative errors of the absorption coefficient if a wrong asymmetry factor g (Henyey-Greenstein function) is assumed in the data analysis.

0.6 and 0.95, we expect errors of less than 5% if the wavelength dependence of the asymmetry factor is ignored in the evaluation.

3.2.3 *Phase function*

In a further study the Henyey-Greenstein function in the simulations was changed to a more realistic one. On the one hand we used the measured phase function of Intralipid 20%[19] and on the other hand the phase function for TiO_2 spheres with a diameter of 7 μm ($n = 2.7$) in epoxy resin ($n = 1.57$) calculated with the Mie theory was applied. The asymmetry factor of both phase functions is $g \approx 0.75$. We calculated simulations with $\mu_s' = 1.0$ mm^{-1}, $n = 1.33$ and varied the absorption coefficient between $2.5 \cdot 10^{-3}$ mm$^{-1} < \mu_a < 1$ mm^{-1}. The absorption coefficient is determined using a calibration polynomial calculated from simulations with the same reduced scattering coefficient, refractive index, and g-factor applying the Henyey-Greenstein phase function. The relative errors of μ_a are shown in Fig. 7. From the reflectance calculated with the Intralipid 20% phase function, which is similar to the Henyey-Greenstein function, the absorption coefficient is determined to be approximately 4% too low for all absorption coefficients. Conversely, for the reflectance calculated with the phase function of the TiO_2 spheres larger relative errors are determined for the absorption coefficient. This is caused by the differences between the Henyey-Greenstein function and the phase function of the TiO_2 spheres that show a peak in backward direction. Especially for large μ_a relative errors up to 30% occur. In summary, in media with Henyey-Greenstein- like phase functions this method provides good results, but when the phase function differs this has to be regarded in the theory.

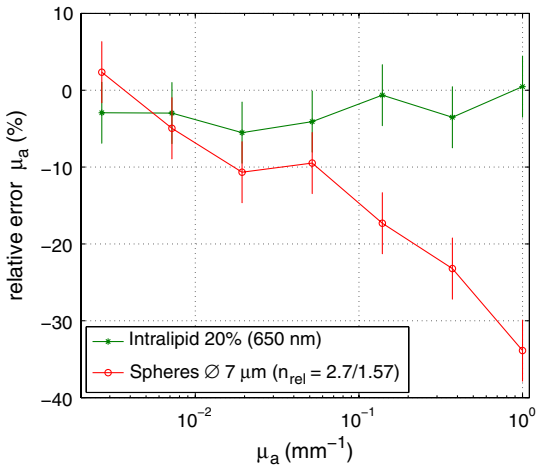

Fig. 7 Relative errors of the absorption coefficient if the reflectance of media having the phase functions of Intralipid 20% (650 nm) or the phase function of TiO_2 spheres (∅ 7 μm) in epoxy resin is evaluated assuming the Henyey-Greenstein function with the same asymmetry factor in the calculations.

4 Measurements on Phantom Media

In order to test the setup, measurements on liquid phantoms made of Intralipid 20%[20,21] (Fresenius Kabi, Bad Homburg, Germany), Ink (Pelikan, black ink, Hannover, Germany), and buffer solution pH 8.0 (Merck, Darmstadt, Germany) were performed. The buffer was used in the phantoms to stabilize the absorber avoiding a spectral shift of the absorption band when the pH changes. In contrast to India ink (suspended carbon particles) the used ink is a solution of different dyes. As it is a molecular absorber with negligible scattering, the absorption coefficient was measured with a spectrophotometer (Cary 5000, Varian/Agilent Technologies, Santa Clara, USA) for comparison with the TR measurements. The absorption in the phantom is caused by ink, water,[22,23] and soy oil in the Intralipid 20%.[14]

For this study, five phantoms were produced with a concentration of $c_L = 0.047$ ml/ml of Intralipid 20% resulting in a reduced scattering coefficient of about 1.5 mm^{-1} at 500 nm. The concentration of ink was varied from 0 ml/ml $< c_I <$ 0.025 ml/ml (V1 to V5). The samples were measured in a cylindrical container with 90 mm in diameter and 50 mm in height. Thus, the medium can be considered as optically semi-infinite for the used parameters. For each phantom we determined the wavelength dependent reduced scattering coefficient using the SRR method and fitted the power law equation $\mu_s' = a\lambda^{-b}$ to the values. The determined reduced scattering coefficient is not shown as it fits the power law excellently. The absorption coefficient was calculated using the reduced scattering coefficient measured before as described in Sec. 2.1. In the calibration simulation a constant refractive index of $n = 1.33$ and anisotropy factor of $g = 0.8$ were assumed. Figure 8 shows the determined absorption coefficients of the phantoms together with the expected values. The expected

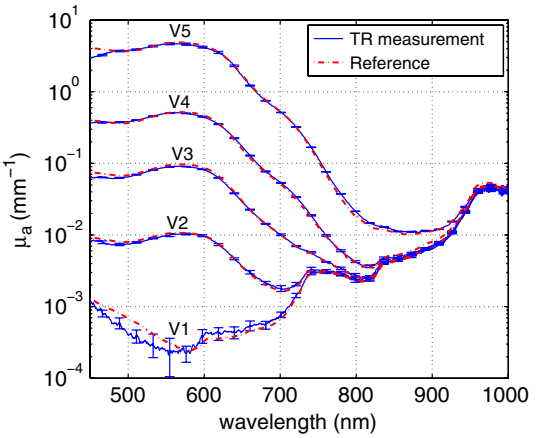

Fig. 8 The determined absorption coefficients of the Intralipd 20% and ink phantoms. The results of the measurement of the TR are compared with the predicted absorption coefficient of the phantoms.

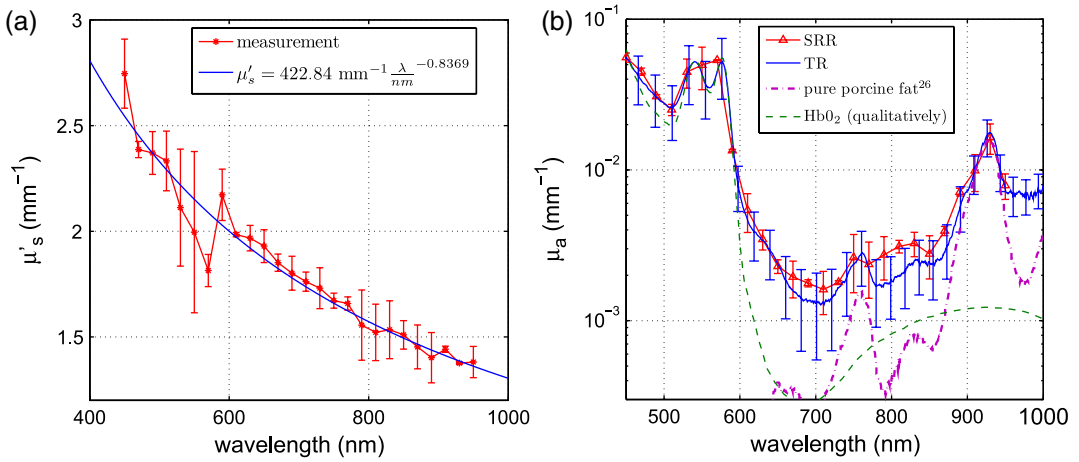

Fig. 9 The reduced scattering coefficient (a) and the absorption coefficient (b) of the fat layer of porcine rind. The comparison with the oxi-haemoglobin and pure porcine fat absorption spectra (b) shows that these substances are main absorbers of the porcine rind.

absorption coefficient is the combination of the water absorption, the soy oil absorption, and the ink absorption considering the concentrations of these absorbers. Each phantom has been measured three times and the standard deviation is represented with error bars. The absorption coefficient determined for the five phantoms agrees well with the predicted absorption spectra. Figure 8 shows that we are able to measure the absorption coefficient over a range of more than four orders of magnitude due to the use of the MC simulations. Large absorption coefficients in comparison with the reduced scattering coefficient can also be determined precisely. The absorption of ink, soy oil, and water can be resolved. Also, with this method the absorption of the Intralipid 20% dilution without ink (V1), as investigated in our earlier paper,[14] can be confirmed. The mean error between the predicted and the determined absorption is lower than 10%.

5 Measurements on Biological Tissue

As one example for measurements on biological tissue we present the determination of μ_s' and μ_a of the fat layer of porcine rind. The skin and the meat have been removed from the rind in order to perform only measurements of the fat layer. As the fat layer from the back of the pig was only approximately 1 cm thick we piled five pieces on top of each other to get a sample of 9 cm × 14 cm by with a height of 5 cm to obtain a optically semi-infinite medium. Because of the softness of the tissue the single pieces fit tightly together without a remaining air gap. Using the SRR method we first determined the reduced scattering and absorption coefficients between 450 and 950 nm with a step size of 20 nm. After interpolating the μ_s' with the power law we determined the absorption coefficient with the TR method again with higher spectral resolution. The results are shown in Fig. 9. For the evaluation a refractive index of $n = 1.46$[24] and an asymmetry factor of $g = 0.8$ were assumed. We performed three measurements on different pieces of the rind. The standard deviation is represented in the error bars. The determined reduced scattering coefficient shows the expected behavior that can be well described by the power law, [see Fig. 9(a)]. The absorption coefficients of the rind measured with both methods show a good agreement within the error bars [compare Fig. 9(b)]. Several features can be observed in the absorption spectrum. In the wavelength range between 500 and 600 nm the absorption of oxi-haemoglobin[25] can be seen. The qualitative comparison with the oxi-haemoglobin spectrum identifies both peaks. Furthermore, the absorption peaks in the spectral range between 700 and 950 nm can be identified as those of pure porcine fat.[26] As the combination of the absorption of oxi-haemoglobin and porcine fat is not identical to the measured spectrum, other absorbers such as deoxi-haemoglobin must be comprised in the fat sample.

6 Conclusion

In summary, we presented a dual step method for the determination of the absorption coefficient of turbid media in a broad spectral range with high spectral resolution. In order to determine the absolute absorption coefficient of turbid media with the measurement of the total reflectance, the knowledge of the reduced scattering coefficient is required. This coefficient was determined with spatially resolved reflectance measurements. The total reflectance was evaluated using MC simulations in which the setup geometry was considered. We showed that the average error of the determined absorption coefficient is smaller than 10%, assuming that the refractive index and the phase function is approximately known for the spectral evaluation. The TR method can be further improved if the wavelength dependence of the refractive index and the phase function is considered in the evaluation. The measurements on Intralipid/ink phantoms verified that the absorption coefficient can be obtained with an average error of less than 10% for a μ_a range of four orders of magnitude. The determination of the absorption coefficient of the fat layer of porcine rind showed absorption peaks that can be associated with the absorption of oxi-haemoglobin and pure porcine fat.

Acknowledgment

We acknowledge the support by the Deutsche Forschungsgemeinschaft (DFG).

References

1. M. Patterson, B. Chance, and B. Wilson, "Time resolved reflectance and transmittance for the non-invasive measurement of tissue optical properties," *Appl. Opt.* **28**(12), 2331–2336 (1989).
2. A. Pifferi et al., "Fully automated time domain spectrometer for the absorption and scattering characterization of diffusive media," *Rev. Sci. Instrum.* **78**(5), 053103 (2007).

3. M. Patterson et al., "Frequency-domain reflectance for the determination of the scattering and absorption properties of tissue," *Appl. Opt.* **30**(31), 4474–4476 (1991).
4. B. Tromberg et al., "Non-invasive measurements of breast tissue optical properties using frequency-domain photon migration," *Phil. Trans. Roy. Soc. Lond. B: Biol. Sci.* **352**(1354), 661–668 (1997).
5. J. Fishkin et al., "Frequency-domain photon migration measurements of normal and malignant tissue optical properties in a human subject," *Appl. Opt.* **36**(1), 10–20 (1997).
6. T. Farrell, M. Patterson, and B. Wilson, "A diffusion theory model of spatially resolved, steady-state diffuse reflectance for the noninvasive determination of tissue optical properties in vivo," *Med. Phys.* **19**(4), 879–888 (1992).
7. A. Kienle et al., "Spatially resolved absolute diffuse reflectance measurements for noninvasive determination of the optical scattering and absorption coefficients of biological tissue," *Appl. Opt.* **35**(13), 2304–2314 (1996).
8. R. Groenhuis, H. Ferwerda, and J. Bosch, "Scattering and absorption of turbid materials determined from reflection measurements. 1: theory," *Appl. Opt.* **22**(16), 2456–2462 (1983).
9. R. Groenhuis, J. Bosch, and H. Ferwerda, "Scattering and absorption of turbid materials determined from reflection measurements. 2: measuring method and calibration," *Appl. Opt.* **22**(16), 2463–2467 (1983).
10. S. Andree et al., "Evaluation of a novel noncontact spectrally and spatially resolved reflectance setup with continuously variable source detector separation using silicone phantoms," *J. Biomed. Opt.* **15**(6), 067009 (2010).
11. M. Nichols, E. Hull, and T. Foster, "Design and testing of a white-light, steady-state diffuse reflectance spectrometer for determination of optical properties of highly scattering systems," *Appl. Opt.* **36**(1), 93–104 (1997).
12. R. Doornbos et al., "The determination of in vivo human tissue optical properties and absolute chromophore concentrations using spatially resolved steady-state diffuse reflectance spectroscopy," *Phys. Med. Biol.* **44**(4), 967–981 (1999).
13. F. Bevilacqua et al., "Broadband absorption spectroscopy in turbid media by combined frequency-domain and steady-state methods," *Appl. Opt.* **39**(34), 6498–6507 (2000).
14. F. Foschum, M. Jäger, and A. Kienle, "Fully automated spatially resolved reflectance spectrometer for the determination of the absorption and scattering in turbid media," *Rev. Sci. Instrum.* **82**(10), 103104 (2011).
15. M. Patterson, E. Schwartz, and B. Wilson, "Quantitative reflectance spectrophotometry for the noninvasive measurement of photosensitizer concentration in tissue during photodynamic therapy," *Proc. SPIE* **1065**, 115–122 (1989).
16. B. Wilson and S. Jacques, "Optical reflectance and transmittance of tissues: principles and applications," *IEEE J. Quant. Electron.* **26**(12), 2186–2199 (1990).
17. L. Wang, S. Jacques, and L. Zheng, "MCML-monte carlo modeling of light transport in multi-layered tissues," *Comput. Meth. Programs Biomed.* **47**(2), 131–146 (1995).
18. L. Henyey and J. Greenstein, "Diffuse radiation in the galaxy," *Astrophys. J.* **93**(1), 70–83 (1941).
19. R. Michels, F. Foschum, and A. Kienle, "Optical properties of fat emulsions," *Opt. Express* **16**(8), 5907–5925 (2008).
20. H. Van Staveren et al., "Light scattering in intralipid-10% in the wavelength range of 400–1100 nm," *Appl. Opt.* **30**(31), 4507–4514 (1991).
21. F. Martelli and G. Zaccanti, "Calibration of scattering and absorption properties of a liquid diffusive medium at NIR wavelengths. cw method," *Opt. Express* **15**(2), 486–500 (2007).
22. L. Kou, D. Labrie, and P. Chylek, "Refractive indices of water and ice in the 0.65-to 2.5-μm spectral range," *Appl. Opt.* **32**(19), 3531–3540 (1993).
23. R. Pope and E. Fry, "Absorption spectrum (380–700 nm) of pure water. ii. integrating cavity measurements," *Appl. Opt.* **36**(33), 8710–8723 (1997).
24. G. Baumert, "Das butter-refraktometer," *Z. Lebensm. Unters. Forsch.* **9**(3), 134–137 (1905).
25. W. Gratzer and A. Allison, "Multiple haemoglobins," *Biol. Rev.* **35**(4), 459–503 (1960).
26. R. Van Veen et al., "Determination of visible near-ir absorption coefficients of mammalian fat using time- and spatially resolved diffuse reflectance and transmission spectroscopy," *J. Biomed. Opt.* **10**(5), 054004 (2005).